Nondipole effects in tunneling ionization by intense laser pulses

Lars Bojer Madsen
Department of Physics and Astronomy, Aarhus University, DK-8000 Aarhus C, Denmark

(Received 24 January 2022; accepted 29 March 2022; published 8 April 2022)

The limit of decreasing laser frequency cannot be considered independently from nondipole effects due to the increase in the laser-induced continuum electron speed in this limit. Therefore, in this work, tunneling ionization in the adiabatic limit is considered for an effective field that includes effects beyond the electric-dipole term to first order in $1/c$, with c being the speed of light. The nondipole term describes the interaction resulting from the electric dipole-induced velocity of the electron and the magnetic-field component of the laser. The impact of this term on the ionization rate, tunnel exit point, momentum at the tunnel exit, and electron dynamics is discussed. In the appropriate limit, the results of a nondipole strong-field approximation approach and those of the strict adiabatic limit, where time and field strength are parameters, are discussed. The nondipole strong-field approximation approach is used to identify nonadiabatic modifications of the initial conditions. The results open up an avenue to include nondipole effects in the initial tunneling ionization step in semiclassical models of strong-field and attosecond physics.

DOI: 10.1103/PhysRevA.105.043107

I. INTRODUCTION

Single ionization of atoms and molecules is the initial key process that triggers a range of dynamics in strong-field and attosecond physics [1,2]. The force on the electron from the field may steer it back to scatter on the parent ion. This laser-driven electron motion may lead to high-harmonic generation, high-energy above-threshold ionization, or multiple ionization [3]. The initial ionization step is also key in the interpretation of, e.g., attoclock experiments [4–6], as well as in time-resolved perspectives on laser-induced electron diffraction [7,8] and strong-field holography [9,10].

When the angular frequency ω of the laser pulse is much smaller than the ionization potential I_p (atomic units are used throughout), the active electron adjusts to the instantaneous value of the electric field such that ionization may be described by static tunneling at an instant in time. This regime is referred to as the strict adiabatic limit, and this is the regime of main consideration in this work. In this regime time and field strength of the laser pulse are parameters in the modeling of the ionization process. As discussed below, the treatment of this limit is complicated by the fact that it cannot be considered independently from a consideration of nondipole effects [11,12].

Setting aside for a moment these latter nondipole-related complications, a typical way to proceed is as follows. After the adiabatic tunneling step, field-induced dynamics take place. These dynamics can be captured by classical considerations [3] and, when including phases along the trajectories, can be used for analysis of interference structures in photoelectron momentum distributions [13,14]. As a result, in the adiabatic regime, semiclassical simulation models, where the first step is quantum-mechanical tunneling and the second is classical propagation from the exit point (a concept justified, e.g., by Bohmian analysis [15]), are among the most used approaches in studying strong-field phenomena. This approach is often referred to as the two-step model when used for ionization. When high-harmonic generation is considered, one uses the word three-step model, where, in the third step, the electron recombines. Tunneling, being the first step in this adiabatic regime, is central in these models, and for this reason there is interest in applying analytical tunneling rate formulas for atoms [16–19] and molecules [20–22]. Modifications of tunneling by permanent dipoles [22,23] and polarizabilities [5,24,25] have also been considered.

Along with the rate, the initial conditions at the tunnel exit are central for the semiclassical simulation. At the tunnel exit, tunneling theory predicts a Gaussian distribution in the momentum transverse to the polarization direction [26], when the field is not too strong [27], and predicts, at the exit point, a vanishing momentum in the longitudinal field (polarization) direction. In particular the latter initial condition has caused some challenges when pursuing agreement between semiclassical models and experimental data. For example, when modeling strong-field ionization at near-infrared fields, it was found that taking a nonvanishing initial value for the longitudinal momentum along the laser polarization direction could sometimes improve the agreement between the semiclassical two-step model and experiment [28–30]. The theoretical justification for such a nonvanishing longitudinal initial momentum is nonexistent in the strict adiabatic tunneling limit, i.e., when tunneling is considered to occur in a field that can be considered static from the point of view of the much faster electronic timescale. However, analytical approaches, which include nonadiabatic effects in the tunneling step, such as the strong-field or Keldysh-Faisal-Reiss approximation [31–33], give predictions for nonvanishing initial momenta along the polarization direction at the tunnel exit when ω is nonvanishing; see the review in [34] for a very thorough discussion

of the Keldysh theory, including discussions of the physical nature of exit points and initial momenta at those points. See also Refs. [35–40] for related theoretical discussions.

In the present work, the situation is elucidated by considering nondipole effects on the ionization rate, tunnel exit, momentum at the tunnel exit, and electron dynamics. According to the Keldysh criterion, the tunneling picture becomes appropriate as $\gamma = \omega\kappa/F_0 \ll 1$ for $\kappa^2/2 = I_p$, where F_0 is the field strength [31]. In this adiabatic limit, one could expect the tunneling description to become increasingly accurate as ω decreases. However, the limit of decreasing ω cannot be considered independently of nondipole effects [11,12]. Namely, when ω decreases, the quiver velocity of the electron F_0/ω increases, and the nondipole effect due to the magnetic-field component of the laser pulse cannot be neglected [11,12]. At first glance, the magnetic component impedes a description in terms of an effective electric-dipole-type interaction, and this could be a reason why analytical descriptions including nondipole effects have applied the strong-field approximation (SFA) approach (see, e.g., Refs. [41–46]).

It is the purpose of this work to deal with nondipole effects in tunneling caused by intense fields ($\sim 10^{14}$ W/cm^2) and to discuss how tunneling concepts can be applied for a suitably defined effective nondipole field in the nonrelativistic, adiabatic regime described by

$$F_0/c \ll \omega \ll I_p/2. \tag{1}$$

The latter inequality ensures that tunneling at the instantaneous field strength is accurate; the factor of $1/2$ is due to the nondipole correction discussed below. Note that in this work, the adiabatic parameter is taken to be $\sim\omega/I_p$. For a discussion of its relation to the Keldysh parameter, see Ref. [47]. As illustrated below, it is possible to have a small Keldysh parameter and at the same time have Eq. (1) fulfilled. The former inequality ensures that nondipole effects are captured by expansion of the vector potential to first order in $1/c$ and that the nondipole SFA Hamiltonian is accurate [48]. Equation (1) applies to atoms and molecules for midinfrared fields at intensities covered by laser sources that are currently being developed [49] and where nondipole effects have been observed [50,51]. In this regime, access to analytical approaches is important for interpretation of data showing signatures of nondipole effects. Note in passing that nondipole effects have also been observed with near-infrared fields [52–56]; see Refs. [57–59] for recent reviews of nondipole effects in intense laser pulses. At near-infrared wavelengths the adiabaticity condition in Eq. (1) is fulfilled to a lesser degree than at midinfrared fields, and therefore, the concept of tunneling at an instantaneous field strength is less valid. Moreover, for a fixed laser intensity, the strong-field nondipole effect decreases with decreasing wavelength since the nondipole term scales as F_0/ω.

This paper is organized as follows. In Sec. II, the theory and the results are presented and discussed. Section III gives the conclusion and an outlook.

II. THEORY AND DISCUSSION

The present analysis will be based on an approximate description of the nondipole effects to order $1/c$. In the high-intensity, high-frequency regime [60–67], it has been known for some time that the leading-order nondipole correction is given by the effect of the magnetic-field component of the laser pulse on the electric-dipole-induced motion of the electron along the laser polarization direction. As detailed in Ref. [48] this interaction is also dominant in intense mid-infrared fields, and the associated Hamiltonian is called the nondipole SFA Hamiltonian [48], where the term SFA refers to the fact that the approximate Hamiltonian is accurate when the field is strong. Equation (1) specifies the condition on ω for the applicability of that approach for a given field strength. This approach was recently applied to laser-assisted scattering [68] and photoelectron momentum distributions [46], in the latter case, leading to conclusions regarding nondipole-induced shifts of momentum distributions that are confirmed by time-dependent Schrödinger equation simulations [45]. For a typical strong laser pulse with a peak intensity of $\sim 10^{14}$ W/cm^2, the nondipole SFA Hamiltonian approach was shown to be accurate in semiclassical modeling at a wavelength of 3400 nm in Ref. [48], and the approach becomes more accurate with increasing wavelength. In the numerical examples below, wavelengths of 3200 and 6400 nm are considered.

A. Nondipole strong-field-approximation Hamiltonian approach

Consider a laser that is linearly polarized along the z direction and propagates along the x direction. For simplicity the pulse is assumed to contain sufficiently many cycles, say, 10 or more, such that the variation of the envelope can be neglected compared with the variation in the carrier. The Hamiltonian with full inclusion of retardation reads

$$H = [\boldsymbol{p} + \boldsymbol{A}(\eta)]^2/2 + V(\boldsymbol{r}), \tag{2}$$

with $V(\boldsymbol{r})$ being the effective single-electron potential and $\eta = \omega t - x\omega/c$. The vector potential is expanded to first order in $1/c$,

$$\boldsymbol{A}(\eta) = \boldsymbol{A}_0(t) + \boldsymbol{A}_1(x,t), \tag{3}$$

with $\boldsymbol{A}_0(t) = \boldsymbol{A}(\eta)|_{\eta=\omega t}$ and $\boldsymbol{A}_1(x,t) = -(\omega x/c)\partial_\eta \boldsymbol{A}(\eta)|_{\eta=\omega t}$. The nondipole SFA Hamiltonian reads [48]

$$H = [\boldsymbol{p} + \boldsymbol{A}_0(t)]^2/2 + \boldsymbol{A}_0(t)\cdot\boldsymbol{A}_1(x,t) + V(\boldsymbol{r}). \tag{4}$$

Compared to the conventional expression for the nondipole Hamiltonian to order $1/c$, the effective Hamiltonian in Eq. (4) neglects the $\boldsymbol{A}_1(x,t)\cdot\boldsymbol{p}$ term. Neglecting this term, compared to the term $\boldsymbol{A}_0(t)\cdot\boldsymbol{A}_1(x,t)$, may be accurate when $\boldsymbol{A}_0(t)$ is large and leads to the nondipole SFA Hamiltonian in Eq. (4). The accuracy of this approach in the long-wavelength, strong-field regime was discuss in detail in Ref. [48]. The nondipole interaction term can be rewritten as

$$\boldsymbol{A}_0(t)\cdot\boldsymbol{A}_1(x,t) = [\dot{\boldsymbol{r}}_{\rm D}\times\boldsymbol{B}_1(t)]\cdot\boldsymbol{r}, \tag{5}$$

where $\dot{\boldsymbol{r}}_{\rm D} = \boldsymbol{A}_0(t)$ is the velocity of the electron in its electric-dipole-induced motion and $\boldsymbol{B}_1(t) = \nabla\times\boldsymbol{A}_1(x,t)$ is the leading-order magnetic field of the laser pulse. Hence, the nondipole term describes the interaction of the electric-dipole-induced motion with the magnetic field. It is noted that the nondipole term on the right-hand side of Eq. (5) is in the form

of an electric dipole operator with an effective field given by

$$\boldsymbol{F}_1(t) = \dot{\boldsymbol{r}}_{\rm D} \times \boldsymbol{B}_1(t) \tag{6}$$

and is directed along the laser propagation direction as per the cross product on the right-hand side of Eq. (6). A unitary transformation changes the entire Hamiltonian in Eq. (4) into the length gauge form, and the result reads

$$H = \frac{p^2}{2} + \tilde{\boldsymbol{F}}(t) \cdot \boldsymbol{r} + V(\boldsymbol{r}), \tag{7}$$

with a nondipole-modified effective field

$$\tilde{\boldsymbol{F}}(t) = \boldsymbol{F}_0(t) + \boldsymbol{F}_1(t). \tag{8}$$

For a vector potential in the form $\boldsymbol{A}(\eta) = \hat{z}A_0\cos(\eta)$, the electric dipole field $\boldsymbol{F}_0(t) = -\partial_t \boldsymbol{A}_0(t)$ reads

$$\boldsymbol{F}_0(t) = \hat{z}F_0(t) = \hat{z}F_0\sin(\omega t), \tag{9}$$

and the nondipole term that follows from the above considerations reads

$$\boldsymbol{F}_1(t) = \hat{\boldsymbol{x}}F_1(t) = \hat{\boldsymbol{x}}\frac{F_0^2}{\omega c}\sin(\omega t)\cos(\omega t) = \hat{\boldsymbol{x}}\frac{F_0^2}{2\omega c}\sin(2\omega t). \tag{10}$$

Equation (7) allows the consideration of nondipole terms in adiabatic tunneling ionization for frequencies fulfilling Eq. (1) due to the presence of the effective field $\tilde{\boldsymbol{F}}(t)$ given by Eq. (8). This effective field has the dipole component along the polarization direction ($\hat{z}$) and the nondipole term along the propagation direction ($\hat{\boldsymbol{x}}$). To illustrate typical $\boldsymbol{F}_0(t)$ and $\boldsymbol{F}_1(t)$ fields, it suffices to consider a quarter of a period from the peak of $\boldsymbol{F}_0(t)$, and Fig. 1(a) shows an example of their magnitudes for midinfrared wavelengths. The oscillation at 2ω in Eq. (10) explains the factor of $1/2$ in Eq. (1).

B. Strict adiabatic limit

In this section, the strict adiabatic limit is considered. In this limit the time of ionization, denoted by t_0, and therefore the field strength of the laser pulse are considered as parameters, and the tunneling is assumed to occur at an instantaneous value of the field. This means that the process takes place for finite, small ω and not too high F_0 to conform to the restrictions set by Eq. (1). It may be helpful to consider some typical numerical values for the quantities that enter Eq. (1). For example, at an intensity of 10^{14} W/cm^2 the left-hand side of Eq. (1) equals 3.9×10^{-4}, and for typical atoms the right-hand side is around 0.2. The angular frequencies for 3200- and 6400-nm light are 1.4×10^{-2} and 7.1×10^{-3}, respectively, which are both within the ω range specified by Eq. (1). The Keldysh parameters for these two cases are 0.27 and 0.14, respectively, so it is possible to have condition (1) fulfilled and at the same time have a Keldysh parameter that is smaller than unity.

The instantaneous magnitude of the field at the time of ionization $|\tilde{\boldsymbol{F}}(t_0)| = \sqrt{F_0(t_0)^2 + F_1(t_0)^2} \simeq |\boldsymbol{F}_0(t_0)|$ equals the magnitude of the electric dipole part of the field to order $1/c$. Accordingly, to order $1/c$, the tunneling rate to exponential accuracy is unaffected by the nondipole correction and is

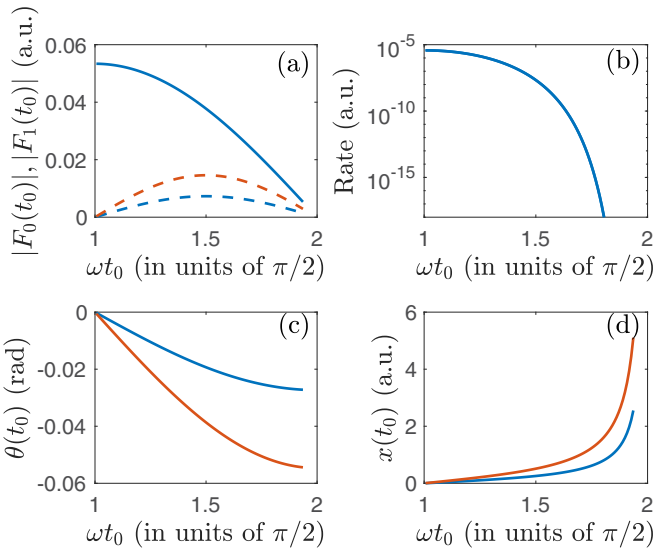

FIG. 1. (a) Norm of electric field $F_0(t_0)$ [Eq. (9), solid blue curve] and $F_1(t_0)$ [Eq. (10), dashed curves] in a half cycle starting from the peak of $F_0(t_0)$ as a function of ionization time t_0. The fields $F_1(t_0)$ are for wavelengths of 3200 (lower dashed blue curve) and 6400 (upper dashed red curve), and they have been multiplied by a factor of 10 for clarity. The maxima in $|F_1(t_0)|$ increase in absolute magnitude for increasing wavelength. The field strength F_0 corresponds to an intensity of 10^{14} W/cm^2. (b) Ionization rate [Eq. (11)] for $F_0(t_0)$ in (a) and $I_p = 0.5$ a.u. (c) Angle $\theta(t_0)$ [Eq. (12)] between the instantaneous direction of the field $\tilde{\boldsymbol{F}}(t_0)$ [Eq. (8)] and the polarization direction for the fields in (a). The amplitude of $\theta(t_0)$ increases with increasing wavelength, 3200 nm for the upper blue curve and 6400 nm for the lower red curve. (d) Position $x(t_0)$ [Eq. (14)] of the exit point in the *propagation* direction for the fields in (a). The amplitude of $x(t_0)$ increases with increasing wavelength, 3200 nm for the lower blue curve and 6400 nm for the upper red curve.

given by the conventional static-field result [16]

$$\Gamma(t_0) \propto \exp\left(-\frac{2\kappa^3}{3|\tilde{\boldsymbol{F}}(t_0)|}\right) \simeq \exp\left(-\frac{2\kappa^3}{3|\boldsymbol{F}_0(t_0)|}\right). \tag{11}$$

Figure 1(b) illustrates this function. While the ionization rate peaks at the peak of $\boldsymbol{F}_0(t_0)$, it is known that rescattering trajectories, crucial for much of strong-field physics, are born over a relatively large interval. For example in Ref. [69], rescattering trajectories with $1.044 \leqslant \omega t_0/(\pi/2) \leqslant 1.278$ [for the present choice of $\boldsymbol{F}_0(t)$] were considered. So even though the ionization rate at, say, $\omega t_0/(\pi/2) \simeq 1.278$ is $\sim 1/3$ of the rate at $\boldsymbol{F}_0(t_0)$ extrema, the corresponding trajectories play a role in dynamics, e.g., at high final kinetic energies. Since the relative strength of the $\boldsymbol{F}_1(t_0)$ correction increases with time from the field maximum [Fig. 1(a)], the importance of the nondipole correction plays a relatively larger role in rescattering trajectories than in direct electrons. A comparison of Figs. 1(a) and 1(b) shows that ionization at the peak of $\boldsymbol{F}_1(t_0)$ is suppressed compared to ionization at times close to the maximum of $\boldsymbol{F}_0(t_0)$.

In contrast to $\Gamma(t_0)$, the tunnel exit points are affected by $\boldsymbol{F}_1(t_0)$ to order $1/c$. The instantaneous direction of the electric field makes an angle, $\theta(t_0)$, with the polarization axis due to the component along the propagation direction, $\tan[\theta(t_0)] =$

$F_1(t_0)/F_0(t_0) = F_0\cos(\omega t_0)/(\omega c)$, and since $\theta(t_0)$ is small,

$$\theta(t_0) = \frac{F_0\cos(\omega t_0)}{\omega c}. \tag{12}$$

The function $\theta(t_0)$ is illustrated in Fig. 1(c). In the electric dipole approximation, the tunnel exit point can be accurately obtained by working in parabolic coordinates [5,70] since the problem involving the sum of the Coulomb potential and the static-field interaction can be variable separated in these coordinates. Here, to illustrate how the nondipole term shifts the tunnel exit point it suffices to consider the field direction model [70]. The component of the exit point in the polarization direction (opposite the direction of the instantaneous field) at the time of ionization can be estimated by

$$\boldsymbol{r}^{\mathrm{D}}(t_0) \simeq -\hat{\boldsymbol{z}}\frac{I_p}{F_0(t_0)}, \tag{13}$$

and it constitutes the exit point in the electric dipole approximation, as indicated by the superscript D. In the approach including nondipole effects, the time-dependent exit points are estimated by $\theta(t_0)$-dependent projections, and to order $1/c$ the result reads

$$\boldsymbol{r}(t_0) = -\hat{\boldsymbol{z}}\frac{I_p}{F_0(t_0)} - \hat{\boldsymbol{x}}\frac{I_p}{F_0(t_0)}\theta(t_0). \tag{14}$$

Equation (14) shows that the nondipole term induces a nonvanishing exit point along the $\hat{\boldsymbol{x}}$ propagation direction, and Fig. 1(d) illustrates typical magnitudes. In the time-of-birth window for rescattering trajectories ($1.044 \leqslant \omega t_0/(\pi/2) \leqslant 1.278$ [69]), $x(t_0)$ may attain values of the order of 10% of an atomic unit, and this value increases with wavelength, as seen from Eq. (12). Note that the variation in wavelength should be considered while keeping in mind the boundaries defined by Eq. (1).

Since the instantaneous field direction is not exclusively along the polarization direction, but rather at an angle $\theta(t_0)$, the momenta at the tunnel exit are also affected by the nondipole term. If the distribution of the initial momenta at the tunnel exit is modeled by a Gaussian transverse to the instantaneous field direction $w(v_\perp(t_0)) \propto \exp[-\kappa v_\perp(t_0)^2/F_0]$ [26], as is typically done in tunneling-based approaches [14,71], the momenta along the propagation and polarization directions at tunneling may be modeled. For simplicity we consider a case where the initial transverse momentum just after tunneling $v_\perp(t_0)$ is in the plane spanned by the two vectors $\boldsymbol{F}_0(t_0)$ and $\boldsymbol{F}_1(t_0)$ and perpendicular to the instantaneous direction of $\tilde{\boldsymbol{F}}(t_0)$. The initial momentum at the time of tunneling is then $v_x(t_0) = v_\perp(t_0)\cos[\theta(t_0)] \simeq v_\perp(t_0)$ in the propagation direction. In the polarization direction, we obtain $v_z(t_0) = -v_\perp(t_0)\sin[\theta(t_0)] \simeq -v_\perp(t_0)\theta(t_0)$ for a given $v_\perp(t_0)$ from the distribution $w(v_\perp(t_0))$. In this sense, the nondipole term induces an initial component along the longitudinal polarization direction, which is absent in the electric dipole approach in the strict adiabatic limit.

The sensitivity of the electron dynamics to the nondipole-induced changes in the tunnel exit point and momentum at the tunnel exit is considered by classical trajectory calculations with full retardation and action of the atomic potential on the outgoing electron. Figure 2 shows an example of an electron initially in the hydrogenic $1s$ state for a set of laser parameters similar to those used in an experiment reporting nondipole effects in the photoelectron momentum distribution [50] (see the caption of Fig. 2 for laser parameters and initial conditions). The excursion in the propagation direction in the nondipole-induced figure-of-eight motion of the free electron is $\simeq$1, and therefore, the parameters are at the onset of low-frequency nondipole effects [11,12]. Figure 2 shows that there are nondipole-induced changes in the time-dependent positions and velocities along both the polarization and propagation directions due to the nondipole-induced modifications at the tunnel exit. In the example considered in Fig. 2, the inclusion of both the nondipole-induced modification of the longitudinal momentum at the tunnel exit and the modification of the tunnel exit point itself leads to a modification of the dynamics that is different from that obtained by just considering the nondipole-induced spatial displacement of the tunnel exit point. The nondipole-induced changes are most clearly seen in the propagation direction [Figs. 2(b) and 2(d)]. The abrupt changes in the trajectories at a propagation time of around 740 a.u. are due to a revisiting of the core region by the electron; that is, the electron passes the Coulomb singularity very closely. The dynamics of the continuum electron depends sensitively on the initial conditions and the combined effect of the external field and the potential of the residual ion. The full exploration of this large parameter space is beyond the scope

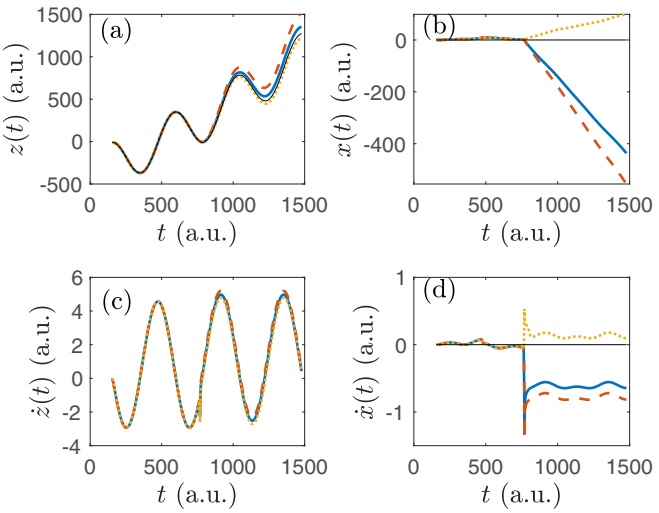

FIG. 2. Illustration of the motion of an electron in a laser field including nondipole effects and a Coulomb potential with unit attractive charge. Position in the (a) polarization and (b) propagation directions. Velocity in the (c) polarization and (d) propagation directions as a function of time. The laser wavelength is 3200 nm, and peak intensity is 10^{14} W/cm^2. The propagation time is three cycles from the peak of the electric dipole field. The solid blue curves show the results for the nondipole exit point [Eq. (14)] and a nonzero choice of the initial $v_x(t_0) = I_p/(3c)$, where the final distribution peaks in the propagation direction [48]. The dashed red curves show results for a dipole exit point and nondipole initial momentum in the propagation direction. The dotted yellow curves show results for the electric dipole exit point [Eq. (13)] and vanishing initial momentum. The thin solid curves show the result for the electric dipole exit point, no initial momentum, and propagation in the electric dipole field. The trajectories are started at $\omega t_0/(\pi/2) = 1.108$ and $I_p = 0.5$ a.u.

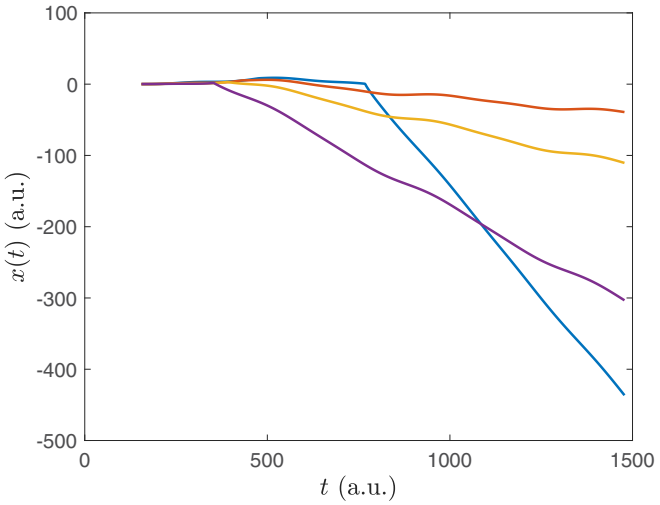

FIG. 3. Position of the electron in the propagation direction as a function of propagation time t after ionization at time t_0 taken as $\omega t_0/(\pi/2) = 1.108$ (blue solid curve from Fig. 2), 1.208 (red, upper curve at large propagation times), 1.308 (yellow, second curve from the top at large propagation times), and 1.408. The plot illustrates the sensitivity to t_0 for the case that takes nondipole exit point and nondipole-induced initial momentum conditions into account. The laser and system parameters are as in Fig. 2.

of the present work. To illustrate the sensitivity to the dynamics of one important parameter, results for dynamics along the propagation direction for different ionization times are shown in Fig. 3. Not surprisingly, there is a relatively large variation in $x(t)$. Such variation is typical for this kind of semiclassical approach, and extensive sampling over initial conditions and appropriately weighted ionization times is needed for quantitative predictions. Still, the main point remains clear: The final momenta can be affected by the nondipole-induced modifications at the tunnel exit, and therefore, these effects should be considered in the interpretation of data, such as holographic and laser-induced diffraction patterns.

C. Nonadiabatic effects of nondipole SFA considerations

The results in this section describe nonadiabatic corrections as captured by the nondipole Volkov phase. The results follow from a nondipole extension of the dipole results discussed, e.g., in Refs. [34,72,73]. It may be useful to stress a fundamental difference compared to the discussion in Sec. II B. In the nondipole SFA approach in the present section, the absence of the atomic potential in the action phase means that there is a simple analytical mapping between initial and final momenta. In contrast, in Sec. II B, the initial conditions are first identified. Then, in the semiclassical approach, forward propagation of the classical equations of motion is performed, and the final momentum for the outgoing electron is obtained through that simulation.

The starting point in this analysis is a consideration of the action phase associated with strong-laser-field ionization in the nondipole-SFA-Hamiltonian approach [46,48],

$$S(t) = \int_{-\infty}^{t} [\boldsymbol{k} + \tilde{\boldsymbol{A}}(t')]^2/2\, dt' + I_p t. \tag{15}$$

Here the factor $I_p t$ comes from the time evolution of the initial bound state, and the momentum $\boldsymbol{k}$ is the asymptotic momentum of the outgoing electron, i.e., the momentum that can be measured at a detector. Now, the integral term comes from the nondipole Volkov phase with the nondipole-modified vector potential

$$\tilde{\boldsymbol{A}}(t) = \boldsymbol{A}_0(t) + \boldsymbol{A}_M(t). \tag{16}$$

Here $\boldsymbol{A}_0(t) = \hat{\boldsymbol{z}} A_0 \cos(\omega t)$, as before, and $\boldsymbol{A}_M(t) = \hat{\boldsymbol{x}} \frac{A_0^2}{2c} \cos^2(\omega t)$ is a $1/c$ nondipole correction to the vector potential which accounts for the dominant effect of the magnetic-field component of the electromagnetic field along the dipole-induced electron trajectories. Clearly, $\boldsymbol{F}_1(t) = -\partial_t \boldsymbol{A}_M(t)$, with $\boldsymbol{F}_1(t)$ being the nondipole-correction field in Eq. (10). Note that the atomic potential does not enter the action of Eq. (15) explicitly; the potential is reflected only through the presence of I_p. This impedes the dependence of the exit point on the spatial variation of the atomic potential. Therefore, the nondipole SFA action-phase approach cannot describe situations in which the exit to the continuum occurs at distances where the atomic potential is not negligible compared to the dipole interaction of the laser field [5]. In the strict adiabatic limit, such a potential effect can be accounted for by improving the approximation leading to Eq. (13), as described in Refs. [5,70]. The effects of the ionic potential on the outgoing electron, including those imparted on the initial conditions, can be taken into account in SFA-related techniques [10].

In the nondipole SFA approach, the notions of (initial) momentum at the tunnel exit and the spatial tunnel exit point come from the consideration of the stationary phase of the action in Eq. (15) with respect to variation in time; that is, they come from the interpretation of the consequences of the condition $\partial_t S(t) = 0$. The latter equation has complex times $t_s = t_0 + i\tau_0$ as solutions. These times are solved as

$$[\boldsymbol{k} + \tilde{\boldsymbol{A}}(t_s)]^2 + \kappa^2 = 0. \tag{17}$$

Inserting the expression for $\tilde{\boldsymbol{A}}(t)$ in Eq. (17) leads to the saddle-point solutions

$$\cos(\omega t_s) = \frac{\omega}{F_0} \left\{ \frac{-k_z \pm i[k_\perp^2 + \kappa^2 + (k^2 + \kappa^2)k_x/c]^{1/2}}{1 + k_x/c} \right\}, \tag{18}$$

with $k_\perp^2 = k_x^2 + k_y^2$ being the momentum transverse to the polarization direction. The real time t_0 is the time of ionization as in Sec. II B. In the dipole approximation, the factor k_x/c goes to zero.

With the complex t_s at hand, the tunnel exit point is found from $\mathrm{Re}[\boldsymbol{r}(t_0)] = \mathrm{Re}\{\int_{t_s}^{t_0} [\boldsymbol{k} + \tilde{\boldsymbol{A}}(t)]dt\}$. The interpretation of this integral is that the electron moves through the effective tunneling barrier in imaginary time from t_s to t_0, i.e., through the complex time interval $t_0 - t_s = -i\tau_0$. An evaluation of the integral gives the tunnel exit point at t_0,

$$\mathrm{Re}[\boldsymbol{r}(t_0)] = \hat{\boldsymbol{z}} \frac{F_0(t_0)}{\omega^2}[1 - \cosh(\omega\tau_0)] + \hat{\boldsymbol{x}} \frac{F_0(t_0)}{4\omega^3 c} F_0 \cos(\omega t_0)\{1 - \cosh[2\omega\tau_0)]\}. \tag{19}$$

Here the nondipole modification of the exit point is the component after the laser propagation direction, $\hat{\boldsymbol{x}}$.

To obtain the momentum at the tunnel exit, consider the condition $\mathrm{Im}[\partial_t S(t)] = 0$. A calculation then shows that the asymptotic longitudinal momentum at the detector k_z can be expressed as

$$k_z = -A_0\left(1 + \frac{k_x}{c}\right)\cos(\omega t_0)\cosh(\omega\tau_0). \tag{20}$$

This relation means that, at the instant of tunneling, the kinematic momentum $\boldsymbol{v}(t_0) = \boldsymbol{k} + \tilde{\boldsymbol{A}}(t_0)$ reads

$$\boldsymbol{v}(t_0) = \hat{\boldsymbol{z}}\frac{F_0}{\omega}\cos(\omega t_0)\left[1 - \left(1 + \frac{k_x}{c}\right)\cosh(\omega\tau_0)\right] + \hat{\boldsymbol{x}}\left[k_x + \frac{F_0^2}{2\omega^2 c}\cos^2(\omega t_0)\right] + \hat{\boldsymbol{y}}k_y. \tag{21}$$

The component along the propagation direction ($\hat{\boldsymbol{x}}$) carries, for fixed intensity, a ω^{-2} scaling. Such a scaling was considered in Ref. [51] to reach agreement between experimental data obtained in the midinfrared regime and the results of a two-step semiclassical simulation including nondipole terms in the propagation of the classical equations of motion after tunneling.

While the expressions in Eqs. (19) and (21) are generally valid within the nondipole SFA approach, a connection to the results obtained in the strict adiabatic limit requires consideration of the limit of small ω in combination with ω fulfilling Eq. (1); see the beginning of Sec. II B for typical numerical values for the quantities entering Eq. (1). To proceed, first, the relation between t_0 and τ_0 is considered. This relation is obtained by using $\mathrm{Re}[\partial_t S(t)] = 0$; that is, the real part of Eq. (17) should be zero. This requirement gives, in combination with Eq. (20),

$$k_\perp^2 + \kappa^2 = \frac{F_0(t_0)^2}{\omega^2}\left(1 + \frac{k_x}{c}\right)\sinh^2(\omega\tau_0) - \frac{F_0^2}{\omega^2}\frac{k_x}{c}\cos^2(\omega t_0)\cosh^2(\omega\tau_0). \tag{22}$$

The relation between t_0 and τ_0 then reads

$$\sinh^2(\omega\tau_0) = \frac{(\omega^2/F_0^2)(k_\perp^2 + \kappa^2) + (k_x/c)\cos^2(\omega t_0)}{(1 + k_x/c)\sin^2(\omega t_0) - (k_x/c)\cos^2(\omega t_0)}, \tag{23}$$

where the k_x-dependent factors on the right-hand side account for the nondipole modification. In the limit of small ω and to first order in $1/c$ it then follows that the dominant contribution to the imaginary part of t_s is given by

$$\cosh(\omega\tau_0) = 1 + \frac{\omega^2(k_\perp^2 + \kappa^2)}{2F_0(t_0)^2}(1 - k_x/c), \tag{24}$$

and therefore,

$$\cosh(2\omega\tau_0) = 1 + \frac{2\omega^2(k_\perp^2 + \kappa^2)}{F_0(t_0)^2}(1 - k_x/c). \tag{25}$$

So in this limit and to first order in $1/c$, Eq. (19) for the tunnel exit point reduces to

$$\mathrm{Re}[\boldsymbol{r}(t_0)] = -\hat{\boldsymbol{z}}\frac{E_\perp + I_p}{F_0(t_0)}(1 - k_x/c) - \hat{\boldsymbol{x}}\frac{E_\perp + I_p}{F_0(t_0)}\theta(t_0). \tag{26}$$

Here $E_\perp = k_\perp^2/2$, and $\theta(t_0)$ is defined in Eq. (12). It is readily seen that the expression in Eq. (26) reduces to the one contained in Eq. (14) in the limit of small longitudinal and transverse momenta.

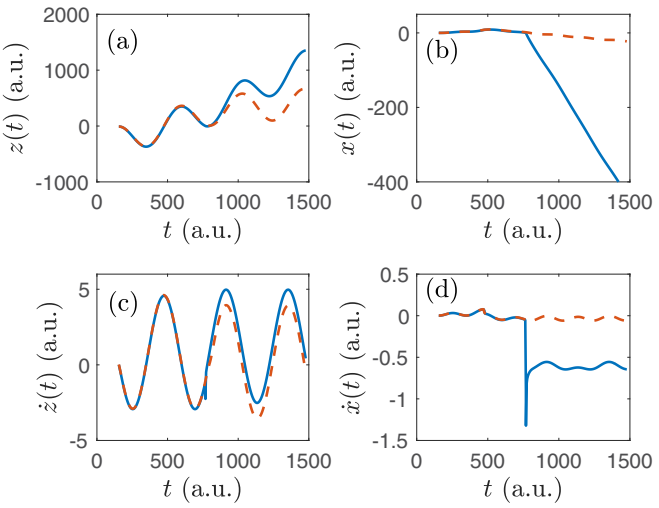

FIG. 4. Illustration of the motion of an electron in a laser field including nondipole and nonadiabatic effects and a Coulomb potential with unit attractive charge. Position in the (a) polarization and (b) propagation directions. Velocity in the (c) polarization and (d) propagation directions as a function of time. The laser parameters and propagation times are as in Fig. 2. The solid blue curves are the same as in Fig. 2 and show the results for the nondipole exit point [Eq. (14)] and a nonzero choice of the initial $v_x(t_0) = I_p/(3c)$, where the final distribution peaks in the propagation direction [48]. The dashed red curves show results when the nonadiabatic corrections in the initial position [Eq. (26)] and initial velocity [Eq. (27)] with $k_x = I_p/(3c)$ are included for $k_y = 0$. The trajectories are started at $\omega t_0/(\pi/2) = 1.108$ and $I_p = 0.5$ a.u.

Regarding the momenta, it is found from Eqs. (21) and (24) that for small ω, the velocity at the exit point at the time of tunneling is connected to the final momentum as follows:

$$\boldsymbol{v}(t_0) = -\hat{\boldsymbol{z}}\theta(t_0)\left(k_x + \frac{c\omega^2(E_\perp + I_p)}{F_0(t_0)^2}\right) + \hat{\boldsymbol{x}}\left[k_x + \frac{F_0^2}{2\omega^2 c}\cos^2(\omega t_0)\right] + \hat{\boldsymbol{y}}k_y. \tag{27}$$

In Eq. (27), the first term $\hat{\boldsymbol{z}}\theta(t_0)k_x$ is similar to the relation discussed in Sec. II B for the initial momentum along the polarization direction with the exception that in Sec. II B the momentum was sampled from a Gaussian distribution of transverse initial momenta at the tunnel exit. Here in the SFA approach, k_x denotes the final momentum at the detector. Any account of the presence of the atomic potential will break the simple relation between final $\boldsymbol{k}$ and initial $\boldsymbol{v}$. The second term along $\hat{\boldsymbol{z}}$ in Eq. (27) is identical to the nonadiabatic correction obtained in the electric dipole approximation (see, e.g., Eq. (5) in Ref. [72]). The expression also accounts for the initial condition along $\boldsymbol{x}$. In this direction, the term proportional to k_x is similar to the one discussed in Sec. II B, again with the difference that in Sec. II B the initial transverse momentum is picked from a Gaussian distribution. The second term along $\hat{\boldsymbol{x}}$ is the nonadiabatic correction. In the numerical examples considered in this work, the nonadiabatic terms in Eq. (27) are larger than the terms proportional to k_x.

From the above results it is seen that in both the strict adiabatic limit and in the case of the nonadiabatic approach with the nondipole Volkov phase, the nondipole correction increases with decreasing ω as $1/\omega$ due to the form of $\theta(t_0)$ [Eq. (12)]. This behavior as a function of ω is different from the dipole result. In the dipole case, the k_x term in the $\hat{z}$ direction in Eq. (27) is absent, and the longitudinal momentum at the tunnel exit is proportional to ω as $\omega \to 0$, as seen from the last factor along the $\hat{z}$ direction in Eq. (27). In considering these limits, the condition imposed by Eq. (1) should, of course, be kept in mind. The requirement of a small quiver velocity F_0/ω compared to the speed of light c means that ω cannot be chosen to be arbitrarily small.

Figure 4 shows an example illustrating, in addition to the nondipole effects of the strict adiabatic limit, the effect of the nonadiabatic terms in the initial conditions, i.e., the effect of including nonadiabatic shifts as in Eqs. (27) and (26). In Fig. 4, the solid blue curves are as in Fig. 2. That is, these results are for the nondipole initial conditions in the strict adiabatic limit in Sec. II B and propagation in the full nondipole field and Coulomb potential. The dashed red curves include the nonadiabatic terms in the initial conditions. The main reason for the difference in the results in the particular realization of Fig. 4 is due to the extra term in the initial velocity in the polarization ($\hat{z}$) direction in Eq. (27) compared to the initial nondipole-modified velocity in the strict adiabatic limit. This extra nonadiabatic term means that the electron does not traverse the Coulomb singularity at a propagation time of around 740 a.u. as it does without this additional nonadiabatic initial offset. A simulation performed under the same conditions but for 6400-nm light showed no effect of including the nonadiabatic terms in the initial conditions. This 6400-nm case is still within the frequency range defined by Eq. (1), and the smaller ω leads to the decrease in the nonadiabatic offsets of the initial conditions.

III. CONCLUSION AND OUTLOOK

In summary, a nondipole correction of order $1/c$ associated with the dipole-induced motion in the magnetic-field component of the laser pulse was considered. The interaction leads to a term that can be interpreted as an additional electric-field component directed along the propagation direction of the laser pulse. In this case, the ionization rate is unaffected by the nondipole contributions to exponential accuracy. The tunnel exit and momentum at the tunnel exit, however, are affected by the nondipole correction. It was illustrated that the nondipole-induced changes in the initial conditions can lead to changes in the electron dynamics and the final momentum distributions. The nonadiabatic modifications of the initial conditions following a treatment with a nondipole SFA approach were also considered. The results of this work outline how to incorporate nondipole effects in the initial tunneling step and associated phase-space initial conditions and hence open the exploration of nondipole strong-field and attosecond physics based on familiar semiclassical two-step ionization and three-step recombination models.

ACKNOWLEDGMENTS

Useful discussions with A. S. Maxwell, H. Stapelfeldt, S. V. B. Jensen, M. M. Lund, and Thomas Hansen are acknowledged. This work was supported by the Independent Research Fund Denmark (Grants No. 9040-00001B and No. 1026-00040B).

[1] T. Brabec and F. Krausz, Intense few-cycle laser fields: Frontiers of nonlinear optics, Rev. Mod. Phys. **72**, 545 (2000).

[2] F. Krausz and M. Ivanov, Attosecond physics, Rev. Mod. Phys. **81**, 163 (2009).

[3] P. B. Corkum, Plasma Perspective on Strong Field Multiphoton Ionization, Phys. Rev. Lett. **71**, 1994 (1993).

[4] P. Eckle, A. N. Pfeiffer, C. Cirelli, A. Staudte, R. Dörner, H. G. Muller, M. Büttiker, and U. Keller, Attosecond ionization and tunneling delay time measurements in helium, Science **322**, 1525 (2008).

[5] A. N. Pfeiffer, C. Cirelli, M. Smolarski, D. Dimitrovski, M. Abu-samha, L. B. Madsen, and U. Keller, Attoclock reveals natural coordinates of the laser-induced tunnelling current flow in atoms, Nat. Phys. **8**, 76 (2012).

[6] A. S. Kheifets, The attoclock and the tunneling time debate, J. Phys. B **53**, 072001 (2020).

[7] T. Zuo, A. D. Bandrauk, and P. B. Corkum, Laser-induced electron diffraction: A new tool for probing ultrafast molecular dynamics, Chem. Phys. Lett. **259**, 313 (1996).

[8] C. I. Blaga, J. Xu, A. D. DiChiara, E. Sistrunk, K. Zhang, P. Agostini, T. A. Miller, L. F. DiMauro, and C. D. Lin, Imaging ultrafast molecular dynamics with laser-induced electron diffraction, Nature (London) **483**, 194 (2012).

[9] Y. Huismans, A. Rouzée, A. Gijsbertsen, J. H. Jungmann, A. S. Smolkowska, P. S. W. M. Logman, F. Lépine, C. Cauchy, S. Zamith, T. Marchenko, J. M. Bakker, G. Berden, B. Redlich, A. F. G. van der Meer, H. G. Muller, W. Vermin, K. J. Schafer, M. Spanner, M. Yu. Ivanov, O. Smirnova, D. Bauer, S. V. Popruzhenko, and M. J. J. Vrakking, Time-resolved holography with photoelectrons, Science **331**, 61 (2011).

[10] C. F. de Morisson Faria and A. S. Maxwell, It is all about phases: Ultrafast holographic photoelectron imaging, Rep. Prog. Phys. **83**, 034401 (2020).

[11] H. R. Reiss, Limits on Tunneling Theories of Strong-Field Ionization, Phys. Rev. Lett. **101**, 043002 (2008).

[12] H. R. Reiss, The tunnelling model of laser-induced ionization and its failure at low frequencies, J. Phys. B **47**, 204006 (2014).

[13] M. Li, J.-W. Geng, H. Liu, Y. Deng, C. Wu, L.-You Peng, Q. Gong, and Y. Liu, Classical-Quantum Correspondence for Above-Threshold Ionization, Phys. Rev. Lett. **112**, 113002 (2014).

[14] N. I. Shvetsov-Shilovski, M. Lein, L. B. Madsen, E. Räsänen, C. Lemell, J. Burgdörfer, D. G. Arbó, and K. Tőkési, Semiclassical two-step model for strong-field ionization, Phys. Rev. A **94**, 013415 (2016).

[15] I. A. Ivanov, C. H. Nam, and K. T. Kim, Exit point in the strong field ionization process, Sci. Rep. **7**, 39919 (2017).
[16] L. D. Landau and E. M. Lifschitz, *Quantum Mechanics*, 3rd ed. (Pergamon, Oxford, 1977).
[17] B. M. Smirnov and M. I. Chibisov, The breaking up of atomic particles by an electric field and by electron collisions, Zh. Eksp. Teor. Fiz. **49**, 841 (1965) [Sov. Phys. JETP **22**, 585 (1966)].
[18] A. M. Perelomov, V. S. Popov, and M. V. Terentev, Ionization of atoms in an alternating electric field, Zh. Eksp. Teor. Fiz. **50**, 1393 [Sov. Phys. JETP **23**, 924 (1966)].
[19] M. V. Ammosov, N. B. Delone, and V. P. Krainov, Tunnel ionization of complex atoms and of atomic ions in an alternating electromagnetic field, Zh. Eksp. Teor. Fiz. **91**, 2008 (1986) [Sov. Phys. JETP **64**, 1191 (1986)].
[20] X. M. Tong, Z. X. Zhao, and C. D. Lin, Theory of molecular tunneling ionization, Phys. Rev. A **66**, 033402 (2002).
[21] R. Murray, M. Spanner, S. Patchkovskii, and M. Yu. Ivanov, Tunnel Ionization of Molecules and Orbital Imaging, Phys. Rev. Lett. **106**, 173001 (2011).
[22] O. I. Tolstikhin, T. Morishita, and L. B. Madsen, Theory of tunneling ionization of molecules: Weak-field asymptotics including dipole effects, Phys. Rev. A **84**, 053423 (2011).
[23] L. Holmegaard, J. L. Hansen, L. Kalhøj, S. L. Kragh, H. Stapelfeldt, F. Filsinger, J. Küpper, G. Meijer, D. Dimitrovski, M. Abu-samha, C. P. J. Martiny, and L. B. Madsen, Photoelectron angular distributions from strong-field ionization of oriented molecules, Nat. Phys. **6**, 428 (2010).
[24] T. Brabec, M. Côté, P. Boulanger, and L. Ramunno, Theory of Tunnel Ionization in Complex Systems, Phys. Rev. Lett. **95**, 073001 (2005).
[25] J. Maurer, D. Dimitrovski, L. Christensen, L. B. Madsen, and H. Stapelfeldt, Molecular-Frame 3D Photoelectron Momentum Distributions by Tomographic Reconstruction, Phys. Rev. Lett. **109**, 123001 (2012).
[26] N. B. Delone and V. P. Krainov, Energy and angular electron spectra for the tunnel ionization of atoms by strong low-frequency radiation, J. Opt. Soc. Am. B **8**, 1207 (1991).
[27] P. A. Batishchev, O. I. Tolstikhin, and T. Morishita, Atomic Siegert states in an electric field: Transverse momentum distribution of the ionized electrons, Phys. Rev. A **82**, 023416 (2010).
[28] A. N. Pfeiffer, C. Cirelli, A. S. Landsman, M. Smolarski, D. Dimitrovski, L. B. Madsen, and U. Keller, Probing the Longitudinal Momentum Spread of the Electron Wave Packet at the Tunnel Exit, Phys. Rev. Lett. **109**, 083002 (2012).
[29] X. Sun, M. Li, J. Yu, Y. Deng, Q. Gong, and Y. Liu, Calibration of the initial longitudinal momentum spread of tunneling ionization, Phys. Rev. A **89**, 045402 (2014).
[30] S. Eckart, K. Fehre, N. Eicke, A. Hartung, J. Rist, D. Trabert, N. Strenger, A. Pier, L. Ph. H. Schmidt, T. Jahnke, M. S. Schöffler, M. Lein, M. Kunitski, and R. Dörner, Direct Experimental Access to the Nonadiabatic Initial Momentum Offset upon Tunnel Ionization, Phys. Rev. Lett. **121**, 163202 (2018).
[31] L. V. Keldysh, Ionization in the field of a strong electromagnetic wave, Zh. Eksp. Teor. Fiz. **47**, 1945 (1964) [Sov. Phys. JETP **20**, 1307 (1965)].
[32] H. R. Reiss, Effect of an intense electromagnetic field on a weakly bound system, Phys. Rev. A **22**, 1786 (1980).
[33] F. H. M. Faisal, Multiple absorption of laser photons by atoms, J. Phys. B **6**, L89 (1973).
[34] S. V. Popruzhenko, Keldysh theory of strong field ionization: history, applications, difficulties and perspectives, J. Phys. B **47**, 204001 (2014).
[35] N. Teeny, E. Yakaboylu, H. Bauke, and C. H. Keitel, Ionization Time and Exit Momentum in Strong-Field Tunnel Ionization, Phys. Rev. Lett. **116**, 063003 (2016).
[36] H. Ni, U. Saalmann, and J.-M. Rost, Tunneling Ionization Time Resolved by Backpropagation, Phys. Rev. Lett. **117**, 023002 (2016).
[37] J. Tian, X. Wang, and J. H. Eberly, Numerical Detector Theory for the Longitudinal Momentum Distribution of the Electron in Strong Field Ionization, Phys. Rev. Lett. **118**, 213201 (2017).
[38] R. Xu, T. Li, and X. Wang, Longitudinal momentum of the electron at the tunneling exit, Phys. Rev. A **98**, 053435 (2018).
[39] H. Ni, U. Saalmann, and J.-M. Rost, Tunneling exit characteristics from classical backpropagation of an ionized electron wave packet, Phys. Rev. A **97**, 013426 (2018).
[40] H. Ni, N. Eicke, C. Ruiz, J. Cai, F. Oppermann, N. I. Shvetsov-Shilovski, and L.-W. Pi, Tunneling criteria and a nonadiabatic term for strong-field ionization, Phys. Rev. A **98**, 013411 (2018).
[41] M. Klaiber, E. Yakaboylu, H. Bauke, K. Z. Hatsagortsyan, and C. H. Keitel, Under-the-Barrier Dynamics in Laser-Induced Relativistic Tunneling, Phys. Rev. Lett. **110**, 153004 (2013).
[42] S. Brennecke and M. Lein, High-order above-threshold ionization beyond the electric dipole approximation: Dependence on the atomic and molecular structure, Phys. Rev. A **98**, 063414 (2018).
[43] S. Brennecke and M. Lein, Strong-field photoelectron holography beyond the electric dipole approximation: A semiclassical analysis, Phys. Rev. A **100**, 023413 (2019).
[44] H. Ni, S. Brennecke, X. Gao, P.-L. He, S. Donsa, I. Březinová, F. He, J. Wu, M. Lein, X.-M. Tong, and J. Burgdörfer, Theory of Subcycle Linear Momentum Transfer in Strong-Field Tunneling Ionization, Phys. Rev. Lett. **125**, 073202 (2020).
[45] S. Brennecke and M. Lein, Nondipole modification of the ac Stark effect in above-threshold ionization, Phys. Rev. A **104**, L021104 (2021).
[46] M. M. Lund and L. B. Madsen, Nondipole photoelectron momentum shifts in strong-field ionization with mid-infrared laser pulses of long duration, J. Phys. B **54**, 165602 (2021).
[47] O. I. Tolstikhin, T. Morishita, and S. Watanabe, Adiabatic theory of ionization of atoms by intense laser pulses: One-dimensional zero-range-potential model, Phys. Rev. A **81**, 033415 (2010).
[48] S. V. B. Jensen, M. M. Lund, and L. B. Madsen, Nondipole strong-field-approximation hamiltonian, Phys. Rev. A **101**, 043408 (2020).
[49] B. Wolter, M. G. Pullen, M. Baudisch, M. Sclafani, M. Hemmer, A. Senftleben, C. D. Schröter, J. Ullrich, R. Moshammer, and J. Biegert, Strong-Field Physics with Mid-IR Fields, Phys. Rev. X **5**, 021034 (2015).
[50] A. Ludwig, J. Maurer, B. W. Mayer, C. R. Phillips, L. Gallmann, and U. Keller, Breakdown of the Dipole Approximation in Strong-Field Ionization, Phys. Rev. Lett. **113**, 243001 (2014).

[51] B. Willenberg, J. Maurer, B. W. Mayer, and U. Keller, Subcycle time resolution of multi-photon momentum transfer in strong-field ionization, Nat. Commun. **10**, 5548 (2019).

[52] C. T. L. Smeenk, L. Arissian, B. Zhou, A. Mysyrowicz, D. M. Villeneuve, A. Staudte, and P. B. Corkum, Partitioning of the Linear Photon Momentum in Multiphoton Ionization, Phys. Rev. Lett. **106**, 193002 (2011).

[53] S. Brennecke and M. Lein, High-order above-threshold ionization beyond the electric dipole approximation, J. Phys. B **51**, 094005 (2018).

[54] N. Haram, I. Ivanov, H. Xu, K. T. Kim, A. Atia-tul-Noor, U. S. Sainadh, R. D. Glover, D. Chetty, I. V. Litvinyuk, and R. T. Sang, Relativistic Nondipole Effects in Strong-Field Atomic Ionization at Moderate Intensities, Phys. Rev. Lett. **123**, 093201 (2019).

[55] A. Hartung, S. Eckart, S. Brennecke, J. Rist, D. Trabert, K. Fehre, M. Richter, H. Sann, S. Zeller, K. Henrichs, G. Kastirke, J. Hoehl, A. Kalinin, M. S. Schöffler, T. Jahnke, L. Ph. H. Schmidt, M. Lein, M. Kunitski, and R. Dörner, Magnetic fields alter strong-field ionization, Nat. Phys. **15**, 1222 (2019).

[56] A. Hartung, S. Brennecke, K. Lin, D. Trabert, K. Fehre, J. Rist, M. S. Schöffler, T. Jahnke, L. Ph. H. Schmidt, M. Kunitski, M. Lein, R. Dörner, and S. Eckart, Electric Nondipole Effect in Strong-Field Ionization, Phys. Rev. Lett. **126**, 053202 (2021).

[57] M.-X. Wang, S.-G. Chen, H. Liang, and L.-Y. Peng, Review on non-dipole effects in ionization and harmonic generation of atoms and molecules, Chin. Phys. B **29**, 013302 (2020).

[58] N. Haram, R. T. Sang, and I. V. Litvinyuk, Transverse electron momentum distributions in strong-field ionization: Nondipole and coulomb focusing effects, J. Phys. B **53**, 154005 (2020).

[59] J. Maurer and U. Keller, Ionization in intense laser fields beyond the electric dipole approximation: Concepts, methods, achievements and future directions, J. Phys. B **54**, 094001 (2021).

[60] A. Bugacov, M. Pont, and R. Shakeshaft, Possibility of breakdown of atomic stabilization in an intense high-frequency field, Phys. Rev. A **48**, R4027(R) (1993).

[61] J. R. Vázquez de Aldana, N. J. Kylstra, L. Roso, P. L. Knight, A. Patel, and R. A. Worthington, Atoms interacting with intense, high-frequency laser pulses: Effect of the magnetic-field component on atomic stabilization, Phys. Rev. A **64**, 013411 (2001).

[62] M. Førre and A. S. Simonsen, Nondipole ionization dynamics in atoms induced by intense xuv laser fields, Phys. Rev. A **90**, 053411 (2014).

[63] A. S. Simonsen and M. Førre, Magnetic-field-induced enhancement of atomic stabilization in intense high-frequency laser fields, Phys. Rev. A **92**, 013405 (2015).

[64] M. Førre and A. S. Simonsen, Generalized velocity-gauge form of the light-matter interaction hamiltonian beyond the dipole approximation, Phys. Rev. A **93**, 013423 (2016).

[65] A. S. Simonsen and M. Førre, Dipole-forbidden atomic transitions induced by superintense x-ray laser fields, Phys. Rev. A **93**, 063425 (2016).

[66] T. E. Moe and M. Førre, Ionization of atomic hydrogen by an intense x-ray laser pulse: An *ab initio* study of the breakdown of the dipole approximation, Phys. Rev. A **97**, 013415 (2018).

[67] M. Førre and S. Selstø, Schrödinger formulation of the nondipole light-matter interaction consistent with relativity, Phys. Rev. A **101**, 063416 (2020).

[68] S. V. B. Jensen and L. B. Madsen, Nondipole effects in laser-assisted electron scattering, J. Phys. B **53**, 195602 (2020).

[69] Z. Chen, A.-T. Le, T. Morishita, and C. D. Lin, Quantitative rescattering theory for laser-induced high-energy plateau photoelectron spectra, Phys. Rev. A **79**, 033409 (2009).

[70] N. I. Shvetsov-Shilovski, D. Dimitrovski, and L. B. Madsen, Ionization in elliptically polarized pulses: Multielectron polarization effects and asymmetry of photoelectron momentum distributions, Phys. Rev. A **85**, 023428 (2012).

[71] Y. Ma, J. Zhou, P. Lu, H. Ni, and J. Wu, Influence of nonadiabatic, nondipole and quantum effects on the attoclock signal, J. Phys. B **54**, 144001 (2021).

[72] M. Li, J.-W. Geng, M. Han, M.-M. Liu, L.-Y. Peng, Q. Gong, and Y. Liu, Subcycle nonadiabatic strong-field tunneling ionization, Phys. Rev. A **93**, 013402 (2016).

[73] E. Pisanty and M. Ivanov, Slalom in complex time: Emergence of low-energy structures in tunnel ionization via complex-time contours, Phys. Rev. A **93**, 043408 (2016).